

Asymmetric Hierarchical Anchoring for Audio–Visual Joint Representation: Resolving Information Allocation Ambiguity for Robust Cross-Modal Generalization

Bixing Wu ^{* 1} Yuhong Zhao ^{* 1} Zongli Ye ^{* 1 2} Jiachen Lian ³ Xiangyu Yue ² Gopala Anumanchipalli ³

Abstract

Audio–visual joint representation learning under Cross-Modal Generalization (CMG) aims to transfer knowledge from a labeled source modality to an unlabeled target modality through a unified discrete representation space. Existing symmetric frameworks often suffer from information allocation ambiguity, where the absence of structural inductive bias leads to semantic–specific leakage across modalities. We propose Asymmetric Hierarchical Anchoring (AHA), which enforces directional information allocation by designating a structured semantic anchor within a shared hierarchy. In our instantiation, we exploit the hierarchical discrete representations induced by audio Residual Vector Quantization (RVQ) to guide video feature distillation into a shared semantic space. To ensure representational purity, we replace fragile mutual information estimators with a GRL-based adversarial decoupler that explicitly suppresses semantic leakage in modality-specific branches, and introduce Local Sliding Alignment (LSA) to encourage fine-grained temporal alignment across modalities. Extensive experiments on AVE and AVVP benchmarks demonstrate that AHA consistently outperforms symmetric baselines in cross-modal transfer. Additional analyses on talking-face disentanglement experiment further validate that the learned representations exhibit improved semantic consistency and disentanglement, indicating the broader applicability of the proposed framework.

1. Introduction

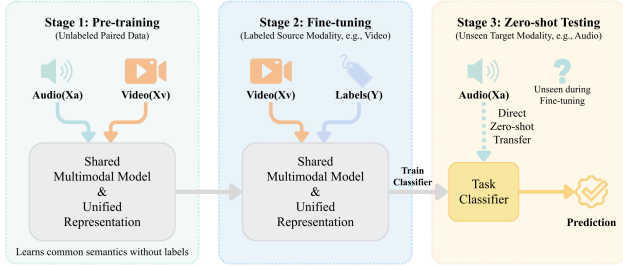


Figure 1. The Cross-Modal Generalization (CMG) Task Definition

Multimodal learning aims to mimic human perceptual integration, driving significant progress in tasks such as Visual Question Answering (Antol et al., 2015; Lei et al., 2018; Li et al., 2022) and Audio–Visual Event Localization (Tian et al., 2018; Xu et al., 2020; Geng et al., 2025). In this work, we focus on audio–visual joint representation learning, where early research predominantly employed implicit continuous representations (e.g., CLIP (Radford et al., 2021), ImageBind (Girdhar et al., 2023)) to align semantics via contrastive learning to reduce the distance between different modalities in high-dimensional semantic space, the field has increasingly shifted towards explicit discrete representations based on codebooks (e.g., (Duan et al., 2022; Liu et al., 2022; Lu et al., 2022; Chen et al., 2025b)) or prototype (Snell et al., 2017; Chen et al., 2023) to represent different modalities. As shown in Figure 2, to mitigate the Modality Gap, a modality-specific branch was introduced, which enables discrete representations to capture cross-modal semantic information. The use of discrete space enables aggregation of similar input features in high-dimensional space, allowing complex feature representations to be achieved with a small number of latent codes. However, existing discretization methods often rely on the idealized assumption of perfect alignment, failing to address the semantic gaps and annotation cost disparities inherent in unconstrained videos. To overcome these limitations, Cross-Modal Generalization (CMG) task and the Unicode framework (Xia et al., 2023) were introduced. This approach achieves fine-grained unified discrete rep-

^{*}Equal contribution ¹Zhejiang University, China ²MMLab, Chinese University of Hong Kong, China ³University of California, Berkeley, USA. Correspondence to: Jiachen Lian <jiachenlian@berkeley.edu>.

resentations on unpaired data, enabling zero-shot transfer capabilities under single-modality training.

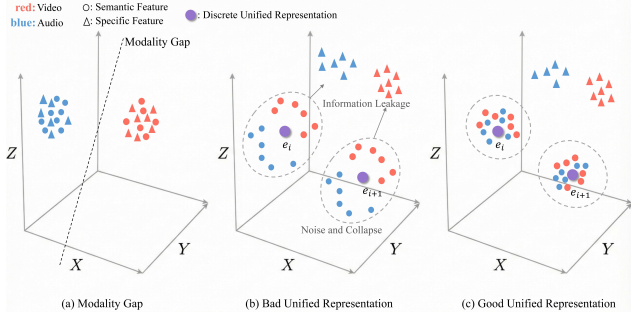


Figure 2. Illustration of the challenges and goals in audio-visual joint representation learning. (a) Modality Gap: Audio (blue) and video (red) features are separated in the latent space due to modality-specific biases. This is why we need to separate the semantic and specific parts; (b) Bad Unified Representation: A naive unification leads to information leakage and semantic codebook collapse, where semantic and modality-specific factors are entangled around discrete codes; (c) Good Unified Representation: A well-structured unified space aligns cross-modal semantic features around shared discrete representations while isolating modality-specific variations.

Although the current explicit representations achieve certain effects on standard downstream tasks, our analysis and experiments show that this does not necessarily mean effective disentanglement of semantic and specific information. In experiments we designed, we find that due to the weak information retention capacity of the previous discrete semantic codebook, the shared space of the symmetric structure undergoes collapse, that is, semantic information tends to flow more towards the specific branches which have less constraints rather than towards the discrete unified representation desired by the CMG task. This exposes potential limitations of the symmetric structure in disentanglement, which we define as Information Allocation Ambiguity. These works (Xia et al., 2023; Huang et al., 2025) often use Mutual Information (MI) estimators, such as the Contrastive Log-ratio Upper Bound (CLUB) (Cheng et al., 2020), to minimize the correlation between the two streams. However, we find that MI minimization via variational upper-bound estimators (e.g., CLUB), which relies on learning a conditional model, becomes unreliable in unconstrained high-dimensional settings.

Our work attempts to answer a more structured question: in audio–visual joint representation, whether semantic information is explicitly concentrated in a designated shared subspace and does not leak into modality-specific branches. This distinction is particularly critical in generative or controllable modeling tasks. To address this, we propose an Asymmetric Hierarchical Anchoring (AHA) structure. Motivated by the fact that audio is commonly used as a conditioning signal in generative settings and often provides

a compact and robust cue for high-level semantics under unconstrained visual noise (Aytar et al., 2016; Narasimhan et al., 2022; Biner et al., 2024; Cheng et al., 2024; Gao et al., 2025), we anchor semantics on the audio modality, utilizing a single-branch Residual Vector Quantization (RVQ) (Lee et al., 2022) structure to construct an asymmetric semantic anchor point. RVQ has been widely adopted in generation and representation learning (especially in audio field) (Défossez et al., 2022; Kim et al., 2024; Zhang et al., 2025; Kim et al., 2025) due to its ability to naturally decompose a signal into a coarse-to-fine hierarchy where the primary quantization layers capture the most salient semantic concepts. We designate this layer as a semantic anchor, forcing the video’s semantic encoder to align with this pre-defined discrete target. This provides a structural prior that guides visual feature distillation, effectively resolving the allocation dilemma. On this basis, we introduce a more effective Gradient Reversal Layer (GRL)-based Adversarial Decoupler. By treating disentanglement as a min-max game, we suppress modality-specific information from the video semantic branch. Finally, we introduce Local Sliding Alignment (LSA) to refine cross-modal alignment at a granular temporal level for unconstrained sequences. This entire structure has been verified as effective through a series of our experiments. Our main contributions are summarized as follows:

- We introduce an Asymmetric architecture that leverages the hierarchical nature of audio RVQ as a structural anchor to provide a stable target for visual semantic distillation.
- We propose a robust GRL-based Adversarial Decoupler that outperforms traditional variational upper-bound MI estimators in separating semantics from modality-specific information.
- We propose a novel Cross-Modal Generalization framework AHA, which has broad application prospects in generative or controllable modeling tasks.

2. Related Works

Multimodal Unified Representations: Recent research on multimodal unified representation has primarily focused on bridging the semantic gap among heterogeneous data. Mainstream approaches typically align modalities by projecting them into a shared latent space (Petridis et al., 2018; Andonian et al., 2022; Sarkar & Etemad, 2024) or employing modal-general encoders for unified cross-modal feature extraction (Chen et al., 2020; Wang et al., 2022a). To further facilitate cross-modal synergy, cross-modal knowledge distillation is widely adopted for implicit information transfer (Sarkar & Etemad, 2024; Huo et al., 2024; Jeong

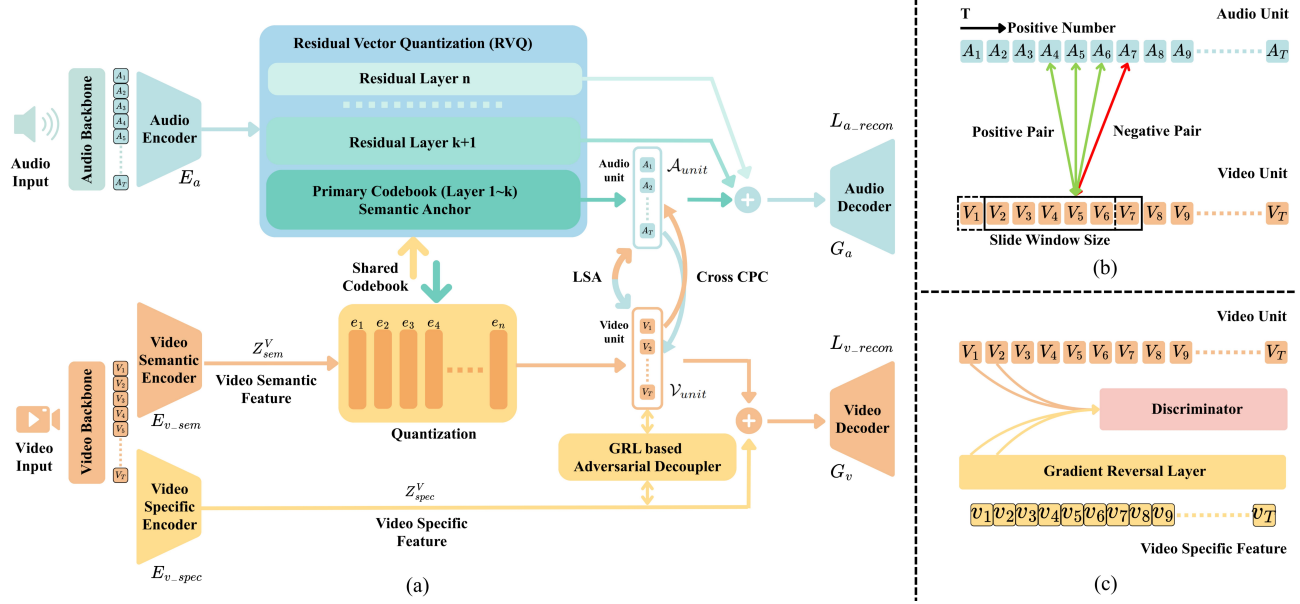


Figure 3. Overview of the proposed AHA architecture. (a) The main pipeline of our entire model. Through our experiments, we found that the effective semantic information in the audio RVQ is generally concentrated in the first two layers. Therefore, we make slight adjustments to k according to the information density required by the task. For the CMG task, to unify the comparison with previous state-of-the-art work, we set $k=1$ by default. For the subsequent Talking Face Disentanglement Experiments Figure 5, we set $k=2$; (b) Framework of Local Sliding Alignment (LSA); (c) Framework of Gradient Reversal Layer(GRL)-based Adversarial Decoupler

et al., 2025), while representation bridging techniques enhance complementarity by connecting distinct continuous spaces (Wang et al., 2023; Grassucci et al., 2025). Furthermore, to enhance interpretability and structure, discretization methods based on codebooks or prototypes have gained increasing attention, mapping continuous features into compact discrete forms (Lu et al., 2022; Jin et al., 2023; Yu et al., 2024).

Mutual Information and GRL Disentanglement: In self-supervised learning, mutual information is commonly used for cross-modal alignment, such as in InfoNCE (Oord et al., 2018), Contrastive Predictive Coding (CPC) (Oord et al., 2018), and MINE (Belghazi et al., 2018), which typically implicitly maximize the mutual information lower bound through contrastive learning or neural estimators. In contrast, for disentanglement between information, variational upper-bound MI estimators like CLUB (Cheng et al., 2020) have difficulty in fitting complex, high-dimensional conditional distributions in unconstrained scenarios. However, in the asymmetric anchor structure we introduced, adversarial learning via Gradient Reversal Layers (GRL) (Ganin & Lempitsky, 2015) benefits from the anchor, offering a more straightforward information stripping paradigm that provides superior robustness in identifying and eliminating biases without complex density estimation and has been applied in many applications (Zhang et al., 2018; Yu et al., 2020; Zhang et al., 2023; Ju et al., 2024). Consequently, we adapt this adversarial paradigm to purge modality-specific

statistics, ensuring a purer semantic space for cross-modal transfer.

3. Method

3.1. Overview and Notations

As illustrated in Figure 3, our framework aligns cross-modal semantics through a dual-stream architecture comprising audio and video branches. Let x_a and x_v denote the input audio and video sequences, respectively. The architecture utilizes three primary encoders: **Audio Encoder** (E_a): Extracts features from the audio input, denoted as the audio backbone output. **Video Semantic Encoder** (E_{v_sem}): Extracts the continuous semantic feature sequence $Z_{sem}^V \in \mathbb{R}^{T \times D}$, which captures high-level content shared across modalities. **Video Specific Encoder** (E_{v_spec}): Extracts the modality-exclusive feature sequence Z_{spec}^V , capturing video-specific attributes.

The core of our alignment strategy is a hierarchical Residual Vector Quantization (RVQ) module containing n layers which is divided into the Primary Codebook (shared semantic anchor) and Residual Specific Layers. After quantization, we obtain the discrete representations $\mathcal{A}_{unit} = \{A_1, \dots, A_T\}$ for audio and $\mathcal{V}_{unit} = \{V_1, \dots, V_T\}$ for video. Finally, the Audio Decoder (G_a) and Video Decoder (G_v) reconstruct the original signals from these disentangled representations.

3.2. Structure of Asymmetric Hierarchical Anchoring

To align cross-modal semantics, we propose Asymmetric Hierarchical Anchoring (AHA), which leverages RVQ’s hierarchical structure to impose directional semantic constraints, enabling consistent alignment without symmetric decomposition.

Shared Semantic Alignment (Layers $1 \sim k$): Due to RVQ’s tendency to aggregate semantic information in lower layers, the first k layers serve as a cross-modal Semantic Anchor. For the audio branch, the input is processed by these shared layers as

$$\mathbf{q}_l = \text{Quantizer}(\mathbf{r}_{l-1}, \mathcal{C}_l \subset \mathcal{C}_{\text{shared}}); \quad l \leq k. \quad (1)$$

where \mathcal{C}_l is the shared codebook at layer l , and \mathbf{r}_{l-1} is the residual from the previous layer (or the input for $l = 1$).

For the video branch, the continuous semantic feature Z_{sem}^V is also projected onto this shared codebook space. This constraint forces the discretized video representation $\mathcal{V}_{\text{unit}}$ to capture only the high-level semantic content that is align with audio semantic and common to both modalities.

Asymmetric Refinement (Layers $k+1 \sim n$): Under the constraint of reconstruction loss, the audio branch extends beyond the shared layers to guide the modality-specific information flow to higher codebooks. The final inputs to the decoders are formulated as:

$$\mathcal{V}_{\text{unit}} = \sum_{l=1}^k \mathbf{q}_l^V; \mathcal{A}_{\text{unit}} = \underbrace{\sum_{l=1}^k \mathbf{q}_l^A}_{\text{Semantic Anchor}} + \underbrace{\sum_{l=k+1}^n \mathbf{q}_l^A}_{\text{Specific features}} \quad (2)$$

3.3. Adversarial Disentanglement via Contrastive Learning

In this section, we elaborate on the adversarial mechanism used to ensure orthogonality between the semantic and specific representations defined in subsection 3.1. Specifically, we aim to ensure that the specific feature Z_{spec}^V extracted by $E_{v,\text{spec}}$ remains independent of the semantic content encapsulated in the Video Units $\mathcal{V}_{\text{unit}}$. To achieve this, we employ a Gradient Reversal Layer (GRL)-based Adversarial Decoupler shown in Figure 3(c).

Adversarial Contrastive Objective: Our objective is to decouple the specific features $v_t \in \mathcal{V}_{\text{spec}}$ and the semantic units $V_t \in \mathcal{V}_{\text{unit}}$. We formulate this as a min-max game involving $E_{v,\text{spec}}$ and a conditional discriminator D_ϕ . The discriminator acts as a critic, attempting to distinguish the matched pair (v_t, V_t) from negative samples. Conversely, $E_{v,\text{spec}}$ aims to deceive the discriminator via the GRL $\mathcal{R}_\lambda(\cdot)$. Let $s(\mathbf{x}, \mathbf{y}) = D_\phi(\mathcal{R}_\lambda(\mathbf{x}), \mathbf{y})$ denote the similarity score. The unified adversarial objective is: $\min_{D_\phi} \max_{E_{v,\text{spec}}} \mathcal{L}_{\text{grl}(adv)} = -\mathbb{E} \left[\log \frac{\exp(s(v, V)/\tau)}{\sum_{V' \in \{\mathcal{V}_{\text{unit}}\} \cup \mathcal{N}} \exp(s(v, V')/\tau)} \right]$ where τ is the temperature and \mathcal{N} denotes the set of negative semantic units.

Velocity-Aware Anchor Sampling: We define the semantic velocity $\delta_t = \|V_{t+1} - V_t\|_2$. The probability of sampling a time step t as an anchor is proportional to its velocity: $P_{\text{sample}}(t) = \frac{\delta_t}{\sum_{\tau} \delta_\tau + \epsilon}$. This ensures the discriminator focuses on dynamic semantic changes rather than static frames. For implementation details, please refer to Algorithm 1.

Algorithm 1 Adversarial Disentanglement with Velocity-Aware Sampling

Require: Video Encoders $E_{v,\text{sem}}, E_{v,\text{spec}}$; Discriminator D_ϕ ; Batch \mathcal{B} .
 Hyperparameters: Max steps N_{max} ; Temp τ ; Smoothing ϵ ; GRL Limit λ_{max} ; Learning rate α ; Model parameters θ .
 Helper Functions: Score $s(\mathbf{x}, \mathbf{y}) = D_\phi([\mathbf{x}, \mathbf{y}])$.
Ensure: Disentangled Specific Features \mathbf{z}_{spec} .
 Initialize step $p \leftarrow 0$
while $p < N_{\text{max}}$ **do**
 1. **Feature Extraction**
 $V \leftarrow \text{Quantizer}(E_{v,\text{sem}}(\mathcal{B})); \{\text{Video Units}\}$
 $v \leftarrow E_{v,\text{spec}}(\mathcal{B}) \{\text{Video Specific Features}\}$
 2. **Velocity-Aware Sampling**
 for each sequence in batch **do**
 $\delta_t \leftarrow \|V_{t+1} - V_t\|_2$
 $P(t) \leftarrow \delta_t / (\sum \delta_\tau + \epsilon);$
 Sample $\mathcal{K} \sim \text{Multinomial}(P(t))$
 $\hat{V}, \hat{v} \leftarrow \text{Gather}(\{V, v\}, \mathcal{K})$
 end **for**
 3. **Adversarial Objective**
 $\lambda \leftarrow \lambda_{\text{max}} \cdot \left(\frac{2}{1 + \exp(-10 \cdot p / N_{\text{max}})} - 1 \right)$
 Sample negatives \mathcal{N} from batch
 $\mathcal{L}_{\text{grl}(adv)} \leftarrow -\log \frac{\exp(s(\hat{v}, \hat{V})/\tau)}{\sum_{V' \in \{V\} \cup \mathcal{N}} \exp(s(\hat{v}, V')/\tau)}$
 4. **Optimization**
 {Update Discriminator (Minimize Loss)}
 $\theta_D \leftarrow \theta_D - \alpha \nabla_{\theta_D} \mathcal{L}_{\text{adv}}$
 {Update Specific Encoder (Maximize Loss via GRL)}
 $\theta_{E_{v,\text{spec}}} \leftarrow \theta_{E_{v,\text{spec}}} + \alpha \lambda \nabla_{\theta_{E_{v,\text{spec}}}} \mathcal{L}_{\text{adv}}$
 $p \leftarrow p + 1$
 end **while**

3.4. Local Sliding Alignment

To handle the inherent asynchrony between visual and acoustic signals in unconstrained scenarios, we propose a Local Sliding Alignment (LSA) mechanism. As illustrated in Figure 3(b), instead of enforcing strict global matching, LSA encourages local synchronization between Audio Units $\mathcal{A}_{\text{unit}}$ and Video Units $\mathcal{V}_{\text{unit}}$. By explicitly modeling local alignment, LSA facilitates more robust cross-modal corre-

spondence under real-world conditions.

We define a Local Search Scope $\Omega_t = \{j \mid |t - j| \leq R\}$ and a Positive Tolerance set $\mathcal{P}_t = \{j \mid |t - j| \leq n_{pos}\}$ (where $n_{pos} \leq R$). We construct a soft-target distribution $Y_{t,j}$ uniformly over \mathcal{P}_t . The predicted alignment probability $P_{t,j}$ is computed via a masked softmax over the audio and video units within Ω_t :

$$Y_{t,j} = \frac{1}{|\mathcal{P}_t|} \mathbb{I}(j \in \mathcal{P}_t), P_{t,j} = \frac{\exp(A_t^\top V_j / \tau)}{\sum_{m \in \Omega_t} \exp(A_t^\top V_m / \tau)} \quad (3)$$

The alignment loss minimizes the bidirectional cross-entropy:

$$\begin{aligned} \mathcal{L}_{align} = -\frac{1}{2T} \sum_{t=1}^T & \left(\sum_{j \in \Omega_t} Y_{t,j} \log P_{t,j}^{A \rightarrow V} \right. \\ & \left. + \sum_{j \in \Omega_t} Y_{t,j} \log P_{t,j}^{V \rightarrow A} \right). \end{aligned} \quad (4)$$

3.5. Fine-Grained Alignment via Cross-CPC and MM-EMA

To bridge the modality gap at a fine-grained level, we employ Cross-Modal Contrastive Predictive Coding (Cross-CPC). We use modality-specific LSTMs to aggregate historical contexts from the quantized units, denoted as \mathbf{h}_t^V and \mathbf{h}_t^A . Crucially, the context of one modality predicts the future semantic units of the counterpart (e.g., \mathbf{h}_t^V predicts A_{t+step}). The symmetric InfoNCE objective is:

$$\begin{aligned} \mathcal{L}_{CPC} &= \frac{1}{2} (\mathcal{L}_{V \rightarrow A} + \mathcal{L}_{A \rightarrow V}), \\ \mathcal{L}_{V \rightarrow A} &\propto - \sum_{t, step} \log \frac{\exp(A_{t+step}^\top W_{step}^V \mathbf{h}_t^V)}{\sum_{A_j \in \mathcal{N}} \exp(A_j^\top W_{step}^V \mathbf{h}_t^V)}. \end{aligned} \quad (5)$$

To encourage feature coupling in the shared latent space, we adopt Multi-Modal Exponential Moving Average (MM-EMA) for codebook updates. Unlike standard EMA, which updates each code vector based on a single modality, MM-EMA aggregates statistics from both audio and video features to ensure that each codebook vector \mathbf{e}_i represents the centroid of the joint distribution.

Specifically, for code i , we maintain a moving average of cluster size N_i and embedding sum \mathbf{m}_i , updated as:

$$\begin{aligned} N_i^{(t)} &= \gamma N_i^{(t-1)} + (1 - \gamma)(n_i^a + n_i^b), \\ \mathbf{m}_i^{(t)} &= \gamma \mathbf{m}_i^{(t-1)} + (1 - \gamma) \left[\sum_{j=1}^{n_i^a} A_{i,j} + \sum_{j=1}^{n_i^b} V_{i,j} \right], \\ \mathbf{e}_i^{(t)} &= \mathbf{m}_i^{(t)} / N_i^{(t)}, \end{aligned} \quad (6)$$

where n_i^a, n_i^b denote the number of features assigned to code i from each modality, and γ is the decay factor.

To further align encoder outputs with these shared centroids, we modify the commitment loss to include both modalities:

$$\mathcal{L}_{commit}^a = \beta \|A_i - \text{sg}[\mathbf{e}_i^a]\|_2^2 + \frac{\beta}{2} \|A_i - \text{sg}[\mathbf{e}_i^b]\|_2^2. \quad (7)$$

The commitment loss for video \mathcal{L}_{commit}^v is defined in the same manner. This approach stabilizes quantization while pulling features from each modality closer to the shared semantic anchors.

3.6. Total Loss Function

The full objective function is a weighted combination of reconstruction, alignment, and disentanglement losses:

$$\begin{aligned} \mathcal{L}_{total} = & L_{a, recon} + L_{v, recon} + \mathcal{L}_{VQ} \\ & + \mathcal{L}_{adv} + \mathcal{L}_{CPC} + \mathcal{L}_{align}, \end{aligned} \quad (8)$$

where $L_{a, recon}$ and $L_{v, recon}$ correspond to the reconstruction losses shown in Figure 3(a), \mathcal{L}_{VQ} sum of the commitment loss from MM-EMA and the commitment loss introduced by the additional audio RVQ layer.

4. Experiment

4.1. Cross-Modality Downstream Tasks

4.1.1. EXPERIMENTAL SETTINGS

Pre-training: We follow Unicode’s CMG evaluation protocol, select the same audio backbone and video backbone, pre-train on unlabeled paired audio–video data, freeze the encoders, train the same linear head using labeled source-modality features and evaluate zero-shot on the target-modality (V→A / A→V). Unless otherwise specified, we use the same single-layer linear classifier and settings as Unicode. Pre-training is conducted on VGGSound-AVEL 40K (Zhou et al., 2021; 2023). (Please see the Appendix A for more implementation details)

Downstream Tasks: We evaluate four standard CMG tasks, each in both transfer directions: **(i) AVE** (Tian et al., 2018): cross-modal event classification on AVE; **(ii) AVVP** (Tian et al., 2020): cross-modal event localization on AVVP; **(iii) AVE → AVVP**: train on AVE classification and evaluate fine-grained localization on AVVP; **(iv) UCF(v) ↔ VGG(a)**: cross-dataset cross-modal classification between UCF-101 (Soomro et al., 2012) (vision) and VGGSound (audio). (Details are shown in Appendix A) We report accuracy for classification tasks and F1 for localization tasks.

Baselines: We compare with MST (You et al., 2022), CODIS (Duan et al., 2022), TURN (Zhao et al., 2022), CMCM (Liu et al., 2022), and Unicode (Xia et al., 2023).

We also report DCID (Huang et al., 2025) and FCID (Huang et al., 2025) as reference results. They use additional text supervision (AVT) during unified-representation pre-training.

Table 1. Cross-modal generalization on downstream CMG tasks. In the tables, $V \rightarrow A$ denotes training with video-modality labels and testing on audio, whereas $A \rightarrow V$ denotes the reverse. **Bold** indicates the best performance, and **blue** denotes the improvement over **Unicode**.

Method	AVE		AVVP		AVE→AVVP		UCF(v)↔VGG(a)		Avg.
	$V \rightarrow A$	$A \rightarrow V$							
MST(AV)	19.5	23.1	22.7	24.5	29.5	36.4	45.7	43.1	30.56
CODIS(AV)	36.8	39.7	32.7	32.6	40.8	40.6	50.8	45.2	39.90
TURN(AV)	37.6	39.2	32.4	32.2	40.6	41.4	50.4	46.1	39.99
CMCM(AV)	46.3	45.8	36.1	35.2	47.1	48.2	51.2	48.3	44.78
Unicode (AV)	49.7	52.3	59.7	63.1	48.9	50.2	64.4	60.6	56.11
DCID(AVT)	54.5	55.0	40.9	41.6	56.5	53.6	68.1	61.7	53.99
FCID(AVT)	55.9	55.0	43.6	45.1	57.4	58.5	69.6	62.0	55.89
Ours (AV)	57.1	59.4	73.4	70.8	52.5	51.3	70.3	63.1	62.24
Improvements	+7.4	+7.1	+13.7	+7.7	+3.6	+1.1	+5.9	+2.5	+6.13

4.1.2. PERFORMANCE ANALYSIS

Table 1 shows that AHA outperforms Unicode on all eight CMG transfer settings, with the largest gains on AVVP, a localization benchmark that is particularly sensitive to fine-grained temporal cross-modal alignment.

Improvements persist under dataset shift ($AVE \rightarrow AVVP$ and $UCF(v) \leftrightarrow VGG(a)$), suggesting that AHA generalizes beyond in-distribution evaluation and can transfer discriminative structure learned on AVE to fine-grained localization on AVVP.

Compared with AVT baselines (DCID/FCID) that use extra text supervision as a stronger semantic bridge across datasets, AHA remains competitive using only audio–video pairs and achieves the best results on AVE/AVVP/UCF(v)↔VGG(a), while AVT methods are stronger on $AVE \rightarrow AVVP$.

Overall, these results suggest that our approach can more effectively extract shared semantics from pure audio–video pairs and support robust cross-modal transfer.

4.2. Ablation Study

Compared with traditional CMG models, AHA differs in three aspects: **(i)** an asymmetric architecture with an audio semantic anchor; **(ii)** GRL-based adversarial decoupler instead of MI-estimation-based decoupler; **(iii)** a local sliding alignment objective for fine-grained temporal alignment. We ablate each component while keeping the CMG protocol and downstream heads unchanged. Since the impact of Cross-CPC and MM-EMA has been discussed in previous work, we do not revisit it here.

Local Sliding Alignment (w/o L_{align}): As shown in **Table 2**, removing L_{align} consistently degrades performance, with

Table 2. Ablation studies on the impact of different loss.

Method	AVE		AVVP		AVE→AVVP		UCF(v)↔VGG(a)		Avg.
	$V \rightarrow A$	$A \rightarrow V$							
Ours	57.1	59.4	73.4	70.8	52.5	51.3	70.3	63.1	62.24
w/o L_{align}	55.4	58.9	65.6	68.1	52.3	51.1	67.6	63.3	60.29
w/o L_{grl}	47.3	50.2	58.1	62.9	49.6	48.2	66.4	61.8	55.56
$L_{grl} \rightarrow L_{CLUB}$	54.2	56.4	64.9	65.5	52.4	50.8	65.1	62.7	59.00

Table 3. Ablation studies on different structures.

Method	AVE		AVVP		AVE→AVVP		UCF(v)↔VGG(a)		Avg.
	$V \rightarrow A$	$A \rightarrow V$							
Ours (audio semantic anchor)	57.1	59.4	73.4	70.8	52.5	51.3	70.3	63.1	62.24
Symmetric audio-video structure	51.5	52.4	70.1	67.4	51.3	51.6	65.4	61.5	58.90
Video semantic anchor	54.7	54.9	69.0	66.1	49.7	48.1	66.5	62.3	58.91

the largest drop on AVVP. This matches our motivation that local sliding alignment provides a tolerant temporal correspondence constraint, sharpening segment-level audio–video matching under small offsets. Notably, the model remains clearly stronger than Unicode even without this term, suggesting that gains are not merely from adding another contrastive loss. Rather, L_{align} mainly refines fine-grained alignment on top of a transferable backbone.

Disentanglement (w/o L_{grl}): Removing GRL-based decoupler causes the largest degradation, especially on AVE and AVVP. Under CMG, the classifier is trained on the source modality only, without explicit disentanglement, modality-identifying cues can leak into the modality-specific branches during source training, creating a pronounced train–test mismatch when transferred to the target modality. These results indicate that L_{grl} is crucial for suppressing modality-specific leakage and enabling reliable zero-shot transfer.

Replacing GRL with CLUB ($L_{grl} \rightarrow L_{CLUB}$): Replacing GRL with CLUB partially recovers the drop but still underperforms the full model, with notable gaps on AVVP. This suggests that GRL-based adversarial decoupler provides a more effective and stable training signal than MI upper-bound minimization.

After validating the contributions of $L_{infonce}$ and GRL disentanglement, we further ablate the architecture along two axes: **(i)** symmetric vs. asymmetric structure; **(ii)** the choice of semantic anchor **Table 3**.

Symmetric vs. Asymmetric: The symmetric dual audio–video structure (Details are shown in [Appendix A](#)) is consistently weaker than our asymmetric design, with clear drops on AVE and $UCF(v) \leftrightarrow VGG(a)$. This is consistent with our analysis of allocation ambiguity, without a directed anchor, semantic information can drift into modality-specific branches, weakening the shared code used for cross-modal transfer.

Choice of Anchor: Within the asymmetric framework, the audio anchor yields the strongest overall transfer and improves most on AVVP, where fine-grained temporal align-

ment is critical. Under dataset shift (AVE \rightarrow AVVP), the video anchor degrades noticeably, while the audio anchor remains substantially higher, the symmetric structure is comparable on A \rightarrow V but is weaker overall due to its larger drops on AVVP. These results support audio anchoring as a directional constraint that reduces semantic allocation ambiguity and yields a more transferable modality-invariant code in CMG tasks.

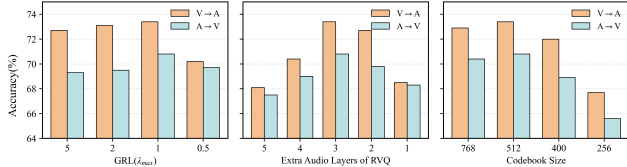


Figure 4. The impact of GRL’s adversarial intensity (larger λ_{max} indicates stronger adversarial effect), RVQ’s number of extra audio layers and Codebook size on experimental accuracy.

4.3. Talking Face Disentanglement Experiment

To address the limitation that previous CMG experiments could only implicitly observe semantic information and disentanglement through data, which lacks intuitiveness, we propose a novel Talking Face Disentanglement Experiment that explicitly tests the model’s disentanglement capability.

Experimental Settings: Based on our original pipeline Figure 3(a), we use the motion encoder from LIA (Wang et al., 2022b; Ki et al., 2025) as the video backbone to extract identity information from the input target video that represents its identity, and extracts video features that contain highly entangled motion information of various facial features. In addition, we use Wav2Vec2.0 (Baevski et al., 2020) as the audio backbone to extract audio features. To better demonstrate the effect of modality transfer, consistent with the CMG experiment approach, we add very sparse phoneme supervision on the time step at the audio shared RVQ side of all models. We selected a filtered TalkVid (Chen et al., 2025a) subset (approximately 30.6 hours) and trained for approximately ten hours on four A6000 GPUs. (Please see the Appendix B for more implementation details)

Expected Results: According to our hypothesis about the Talking Face Disentanglement Experiment, the video information shared with audio should be related to mouth movements, while information representing other facial actions should flow to modality-specific branches. Therefore, the ideal effect of our Talking Face Disentanglement Experiment is to achieve transfer of mouth movements. To elaborate, we can input a semantic video and extract the motion vector representing audio-related mouth movements after passing through the shared RVQ in its pipeline. For another specific video, we can extract the motion vector representing non-mouth movements (such as eye blinking) after passing through the specific encoder in its pipeline. These

two can be concatenated and output, then passed through LIA and concatenated with the target identity information, and rendered through LIA’s renderer. Finally, a fused video is generated that combines the mouth movements from the semantic video and audio-unrelated movements from the specific video. This also validates the model’s decoupling ability, namely whether mixed features common to both videos will appear.

Result Analysis: From Figure 5(a), we can see that our current AHA structure can effectively decouple information, enabling alignment of audio-irrelevant actions (such as eye movements) in specific video and alignment of mouth movements in semantic video, with minimal information leakage. When removing the GRL loss (w/o L_{grl}), the disentanglement effect becomes significantly worse, as evidenced by many cases where mouth movements are closed at the same frame in semantic video, while the frame without GRL has the mouth open, and vice versa. There are also cases where eye movements do not correspond to the corresponding frames in specific video. After replacing GRL with CLUB ($L_{grl} \rightarrow L_{CLUB}$) and retraining, the improvement in overall disentanglement effect is not obvious. This demonstrates that variational MI estimators are weaker than GRL in handling information disentanglement in such complex information environments. For the symmetric structure, despite strong decoupling with GRL, the lack of audio as an anchor point for semantic information causes most information to leak into the modality-specific branches, resulting in poor disentanglement performance.

4.3.1. FURTHER ANALYSIS

Table 4. Quantitative comparison in Visual-to-Visual Lip Synchronization (V2V-LS) and Mouth Landmark RMSE.

	Ours	w/o L_{grl}	$L_{grl} \rightarrow L_{CLUB}$	Symmetric
V2V-LS \downarrow	5.98	6.77	6.82	6.40
Mouth RMSE \downarrow	5.51	16.59	18.26	14.61

Table 5. Quantitative comparison in Peak Signal-to-Noise Ratio (PSNR) and Learned Perceptual Image Patch Similarity (LPIPS)

	Ours	w/o L_{grl}	$L_{grl} \rightarrow L_{CLUB}$	Symmetric
PSNR \uparrow	29.42	26.46	27.49	26.76
LPIPS \downarrow	0.0468	0.0703	0.0575	0.0730

PCA reflects global variance directions. As shown in Figure 5, AHA yields clearly different variance patterns with limited overlap between semantic and specific features, suggesting reduced linear dependency and weaker cross-branch leakage. In contrast, removing GRL or replacing it with CLUB exhibit heavier overlap, indicating that the two branches still share major variation directions. For the symmetric structure, PCA is dominated by the higher-variance branch, compressing the other into a narrow region, which



Figure 5. (a) Talking Face Disentanglement Experiment Results: We selected two videos from sources not in the training set to demonstrate the effect. To better showcase the experimental results, we selected frames where Specific Video and Semantic Video have significant differences (for example: whether eyes are closed and mouth is open) for comparison. We set the identity information as the corresponding identity vector from the Semantic Video. For comparison, we also tested (i) removing GRL from our asymmetric structure (w/o L_{grl}). (ii) replacing GRL with CLUB in the asymmetric structure($L_{grl} \rightarrow L_{CLUB}$). (iii) adding GRL to a symmetric structure identical to Unicode (Symmetric). (Please see the [Appendix B](#) for more experimental results); (b) PCA & UMAP Results: For the same selected video features, we extracted specific features and semantic features, and performed Principal Component Analysis (PCA) and Uniform Manifold Approximation and Projection (UMAP)

is consistent with feature collapse imbalance rather than structural disentanglement.

UMAP mainly preserves local neighborhood structures. Under AHA, semantic and specific features show more separated neighborhoods and distinct manifold shapes, implying that the two branches encode different underlying factors. When removing GRL or replacing it with CLUB, the two features become highly mixed in local neighborhoods and form similar manifold backbones, indicating stronger information leakage. For the symmetric setting, UMAP often produces elongated outliers, again suggesting a distorted neighborhood graph caused by collapse.

We also evaluate video-to-video lip synchronization using V2V-LS and Mouth RMSE (between fused video and semantic video), as shown in [Table 4](#). V2V-LS is designed to measure frame-wise semantic embedding ([Shi et al., 2022](#)) differences of the lip region, while Mouth RMSE quantifies geometric misalignment of 2D mouth landmarks. AHA consistently achieves higher V2V-LS and lower Mouth RMSE compared to other structure, indicating improved the completeness and coherence of semantic information. In addition, we combine the visual semantic and specific feature to reconstruct the original input and then turn it to the full video, as shown in [Table 5](#), AHA achieves the highest PSNR and the lowest LPIPS, outperforming the symmetric baseline and the asymmetric structure without the GRL-based adversarial decoupler. These results indicate that AHA im-

proves reconstruction fidelity and perceptual quality while maintaining effective disentanglement, thereby preserving richer information. Detailed definitions of these metrics are provided in [Appendix B](#).

5. Conclusion

This paper investigates audio-visual joint representation learning under Cross-Modal Generalization (CMG), noting that current symmetric discrete unified representation frameworks are prone to information allocation ambiguity. We propose Asymmetric Hierarchical Anchoring (AHA), leveraging the hierarchical structure of audio RVQ to construct shared semantic anchors guiding directed distillation of video semantic features into a shared codebook, introducing a GRL-based adversarial decoupler to suppress semantic information leakage, and Local Sliding Alignment (LSA) for fine-grained temporal alignment across modalities. Extensive experiments show that AHA outperforms baselines on AVE, AVVP, and cross-dataset transfer, with notable improvements on alignment-sensitive AVVP. We also propose a Talking Face Disentanglement Experiment, validating AHA’s strong decoupling capability and higher reconstruction quality.

Future Work: We plan to study adaptive anchor selection across tasks and extend AHA to more modalities, with systematic evaluations under open-domain noise and long temporal contexts.

Impact Statement

We plan to open-source our code once the paper is accepted, to support transparency and verification of our findings. This work studies audio–visual joint representation learning under Cross-Modal Generalization (CMG) and evaluates disentanglement using a Talking Face Disentanglement Experiment that renders a fused video by combining mouth-related motion from one sequence with other facial motions from another sequence through an existing renderer.

This research may have positive impacts by improving robustness of audio–visual learning under modality shift and reducing reliance on extensive labeled data, potentially benefiting downstream audio–visual understanding and localization tasks.

However, because our evaluation includes generating rendered talking-face videos, parts of the pipeline could be misused to facilitate synthetic media manipulation (e.g., impersonation or non-consensual deepfakes). The societal risks of deepfakes have been discussed in prior surveys (Mirsky & Lee, 2021). To mitigate these risks, we encourage (i) using data with appropriate consent and governance, (ii) clearly disclosing and labeling synthetic outputs, (iii) considering controlled release practices and safety evaluations prior to deployment. We strongly condemn any malicious use of this line of work and advocate responsible and ethical use.

References

Andonian, A., Chen, S., and Hamid, R. Robust cross-modal representation learning with progressive self-distillation. In *Proceedings of the IEEE/CVF Conference on Computer Vision and Pattern Recognition*, pp. 16430–16441, 2022.

Antol, S., Agrawal, A., Lu, J., Mitchell, M., Batra, D., Zitnick, C. L., and Parikh, D. Vqa: Visual question answering. In *Proceedings of the IEEE international conference on computer vision*, pp. 2425–2433, 2015.

Aytar, Y., Vondrick, C., and Torralba, A. Soundnet: Learning sound representations from unlabeled video. *Advances in neural information processing systems*, 29, 2016.

Baevski, A., Zhou, Y., Mohamed, A., and Auli, M. wav2vec 2.0: A framework for self-supervised learning of speech representations. *Advances in neural information processing systems*, 33:12449–12460, 2020.

Belghazi, M. I., Baratin, A., Rajeshwar, S., Ozair, S., Ben-gio, Y., Courville, A., and Hjelm, D. Mutual information neural estimation. In *International conference on machine learning*, pp. 531–540. PMLR, 2018.

Biner, B. C., Sofian, F. M., Karakaş, U. B., Ceylan, D., Erdem, E., and Erdem, A. Sonicdiffusion: Audio-driven image generation and editing with pretrained diffusion models. *arXiv preprint arXiv:2405.00878*, 2024.

Chen, D., Wu, Z., Liu, F., Yang, Z., Zheng, S., Tan, Y., and Zhou, E. Protoclip: Prototypical contrastive language image pretraining. *IEEE Transactions on Neural Networks and Learning Systems*, 2023.

Chen, S., Huang, H., Liu, Y., Ye, Z., Chen, P., Zhu, C., Guan, M., Wang, R., Chen, J., Li, G., et al. Talkvid: A large-scale diversified dataset for audio-driven talking head synthesis. *arXiv preprint arXiv:2508.13618*, 2025a.

Chen, Y.-C., Li, L., Yu, L., El Kholy, A., Ahmed, F., Gan, Z., Cheng, Y., and Liu, J. Uniter: Universal image-text representation learning. In *European conference on computer vision*, pp. 104–120. Springer, 2020.

Chen, Z., Wang, C., Chen, X., Xu, H., Huang, R., Zhou, J., Han, J., Xu, H., and Liang, X. Semhitok: A unified image tokenizer via semantic-guided hierarchical codebook for multimodal understanding and generation. *arXiv preprint arXiv:2503.06764*, 2025b.

Cheng, H., Lin, L., Liu, C., Xia, P., Hu, P., Ma, J., Du, J., and Pan, J. Dawn: Dynamic frame avatar with non-autoregressive diffusion framework for talking head video generation. *arXiv preprint arXiv:2410.13726*, 2024.

Cheng, P., Hao, W., Dai, S., Liu, J., Gan, Z., and Carin, L. Club: A contrastive log-ratio upper bound of mutual information. In *International conference on machine learning*, pp. 1779–1788. PMLR, 2020.

Chung, J. S. and Zisserman, A. Out of time: automated lip sync in the wild. In *Asian conference on computer vision*, pp. 251–263. Springer, 2016.

Défossez, A., Copet, J., Synnaeve, G., and Adi, Y. High fidelity neural audio compression. *arXiv preprint arXiv:2210.13438*, 2022.

Duan, J., Chen, L., Tran, S., Yang, J., Xu, Y., Zeng, B., and Chilimbi, T. Multi-modal alignment using representation codebook. In *Proceedings of the IEEE/CVF Conference on Computer Vision and Pattern Recognition (CVPR)*, pp. 15651–15660, June 2022.

Ganin, Y. and Lempitsky, V. Unsupervised domain adaptation by backpropagation. In *International conference on machine learning*, pp. 1180–1189. PMLR, 2015.

Gao, X., Hu, L., Hu, S., Huang, M., Ji, C., Meng, D., Qi, J., Qiao, P., Shen, Z., Song, Y., et al. Wan-s2v: Audio-driven cinematic video generation. *arXiv preprint arXiv:2508.18621*, 2025.

Geng, T., Wang, T., Duan, J., Zhang, Y., Guan, W., Zheng, F., and Shao, L. Uniav: Unified audio-visual perception for multi-task video event localization. *IEEE Transactions on Pattern Analysis and Machine Intelligence*, 2025.

Girdhar, R., El-Nouby, A., Liu, Z., Singh, M., Alwala, K. V., Joulin, A., and Misra, I. Imagebind: One embedding space to bind them all. In *Proceedings of the IEEE/CVF conference on computer vision and pattern recognition*, pp. 15180–15190, 2023.

Grassucci, E., Cicchetti, G., and Comminiello, D. Closing the modality gap enables novel multimodal learning applications. In *Second Workshop on Representational Alignment at ICLR 2025*, 2025.

Hempel, T., Abdelrahman, A. A., and Al-Hamadi, A. 6d rotation representation for unconstrained head pose estimation. In *2022 IEEE International Conference on Image Processing (ICIP)*, pp. 2496–2500. IEEE, 2022.

Horé, A. and Ziou, D. Image quality metrics: Psnr vs. ssim. In *2010 20th International Conference on Pattern Recognition*, pp. 2366–2369, 2010. doi: 10.1109/ICPR.2010.579.

Huang, H., Xia, Y., Ji, S., Wang, S., Wang, H., Fang, M., Zhu, J., Dong, Z., Zhou, S., and Zhao, Z. Enhancing multimodal unified representations for cross modal generalization. In *Findings of the Association for Computational Linguistics: ACL 2025*, pp. 2353–2366, July 2025. doi: 10.18653/v1/2025.findings-acl.119.

Huo, F., Xu, W., Guo, J., Wang, H., and Guo, S. C2kd: Bridging the modality gap for cross-modal knowledge distillation. In *Proceedings of the IEEE/CVF Conference on Computer Vision and Pattern Recognition*, pp. 16006–16015, 2024.

Jeong, J., Lee, S., Park, D., Lee, G., and Yoon, K.-J. Multi-modal knowledge distillation-based human trajectory forecasting. In *Proceedings of the Computer Vision and Pattern Recognition Conference*, pp. 24222–24233, 2025.

Jin, Y., Xu, K., Chen, L., Liao, C., Tan, J., Huang, Q., Chen, B., Lei, C., Liu, A., Song, C., et al. Unified language-vision pretraining in llm with dynamic discrete visual tokenization. *arXiv preprint arXiv:2309.04669*, 2023.

Ju, Z., Wang, Y., Shen, K., Tan, X., Xin, D., Yang, D., Liu, Y., Leng, Y., Song, K., Tang, S., et al. Naturalspeech 3: Zero-shot speech synthesis with factorized codec and diffusion models. *arXiv preprint arXiv:2403.03100*, 2024.

Ki, T., Min, D., and Chae, G. Float: Generative motion latent flow matching for audio-driven talking portrait. In *Proceedings of the IEEE/CVF International Conference on Computer Vision*, pp. 14699–14710, 2025.

Kim, H., Lee, J., Morton, J., Lee, J., and Yang, J. Improving test-time performance of rvq-based neural codecs. *arXiv preprint arXiv:2509.19186*, 2025.

Kim, J., Moon, T., Lee, K., and Cho, J. Efficient generative modeling with residual vector quantization-based tokens. *arXiv preprint arXiv:2412.10208*, 2024.

Lee, D., Kim, C., Kim, S., Cho, M., and Han, W.-S. Autoregressive image generation using residual quantization. In *Proceedings of the IEEE/CVF conference on computer vision and pattern recognition*, pp. 11523–11532, 2022.

Lei, J., Yu, L., Bansal, M., and Berg, T. Tvqa: Localized, compositional video question answering. In *Proceedings of the 2018 conference on empirical methods in natural language processing*, pp. 1369–1379, 2018.

Li, G., Wei, Y., Tian, Y., Xu, C., Wen, J.-R., and Hu, D. Learning to answer questions in dynamic audio-visual scenarios. In *Proceedings of the IEEE/CVF conference on computer vision and pattern recognition*, pp. 19108–19118, 2022.

Liu, A., Jin, S., Lai, C.-I., Rouditchenko, A., Oliva, A., and Glass, J. Cross-modal discrete representation learning. In *Proceedings of the 60th Annual Meeting of the Association for Computational Linguistics (Volume 1: Long Papers)*, pp. 3013–3035, May 2022. doi: 10.18653/v1/2022.acl-long.215.

Lu, J., Clark, C., Zellers, R., Mottaghi, R., and Kembhavi, A. Unified-io: A unified model for vision, language, and multi-modal tasks. *arXiv preprint arXiv:2206.08916*, 2022.

Mirsky, Y. and Lee, W. The creation and detection of deep-fakes: A survey. *ACM computing surveys (CSUR)*, 54(1): 1–41, 2021.

Narasimhan, M., Ginosar, S., Owens, A., Efros, A. A., and Darrell, T. Strumming to the beat: Audio-conditioned contrastive video textures. In *Proceedings of the IEEE/CVF Winter Conference on Applications of Computer Vision*, pp. 3761–3770, 2022.

Oord, A. v. d., Li, Y., and Vinyals, O. Representation learning with contrastive predictive coding. *arXiv preprint arXiv:1807.03748*, 2018.

Petridis, S., Stafylakis, T., Ma, P., Tzimiropoulos, G., and Pantic, M. Audio-visual speech recognition with a hybrid ctc/attention architecture. In *2018 IEEE Spoken Language Technology Workshop (SLT)*, pp. 513–520. IEEE, 2018.

Prajwal, K., Mukhopadhyay, R., Namboodiri, V. P., and Jawahar, C. A lip sync expert is all you need for speech

to lip generation in the wild. In *Proceedings of the 28th ACM international conference on multimedia*, pp. 484–492, 2020.

Radford, A., Kim, J. W., Hallacy, C., Ramesh, A., Goh, G., Agarwal, S., Sastry, G., Askell, A., Mishkin, P., Clark, J., et al. Learning transferable visual models from natural language supervision. In *International conference on machine learning*, pp. 8748–8763. PMLR, 2021.

Rehman, A., Cai, J., Zhang, J.-J., and Yang, X. Bfa: Real-time multilingual text-to-speech forced alignment. *arXiv preprint arXiv:2509.23147*, 2025.

Sarkar, P. and Etemad, A. Xkd: Cross-modal knowledge distillation with domain alignment for video representation learning. In *Proceedings of the AAAI Conference on Artificial Intelligence*, volume 38, pp. 14875–14885, 2024.

Shi, B., Hsu, W.-N., Lakhotia, K., and Mohamed, A. Learning audio-visual speech representation by masked multimodal cluster prediction. *arXiv preprint arXiv:2201.02184*, 2022.

Snell, J., Swersky, K., and Zemel, R. Prototypical networks for few-shot learning. *Advances in neural information processing systems*, 30, 2017.

Soomro, K., Zamir, A. R., and Shah, M. Ucf101: A dataset of 101 human actions classes from videos in the wild. *arXiv preprint arXiv:1212.0402*, 2012.

Tian, Y., Shi, J., Li, B., Duan, Z., and Xu, C. Audio-visual event localization in unconstrained videos. In *Proceedings of the European Conference on Computer Vision (ECCV)*, September 2018.

Tian, Y., Li, D., and Xu, C. Unified multisensory perception: Weakly-supervised audio-visual video parsing. In *Computer Vision – ECCV 2020*, pp. 436–454, 2020.

Wang, T., Jiang, W., Lu, Z., Zheng, F., Cheng, R., Yin, C., and Luo, P. Vlmixer: Unpaired vision-language pre-training via cross-modal cutmix. In *International Conference on Machine Learning*, pp. 22680–22690. PMLR, 2022a.

Wang, Y., Yang, D., Bremond, F., and Dantcheva, A. Latent image animator: Learning to animate images via latent space navigation. *arXiv preprint arXiv:2203.09043*, 2022b.

Wang, Z., Zhao, Y., Huang, H., Liu, J., Yin, A., Tang, L., Li, L., Wang, Y., Zhang, Z., and Zhao, Z. Connecting multi-modal contrastive representations. *Advances in Neural Information Processing Systems*, 36:22099–22114, 2023.

Xia, Y., Huang, H., Zhu, J., and Zhao, Z. Achieving cross modal generalization with multimodal unified representation. In *Advances in Neural Information Processing Systems*, volume 36, pp. 63529–63541, 2023.

Xu, H., Zeng, R., Wu, Q., Tan, M., and Gan, C. Cross-modal relation-aware networks for audio-visual event localization. In *Proceedings of the 28th ACM international conference on multimedia*, pp. 3893–3901, 2020.

You, H., Zhou, L., Xiao, B., Codella, N., Cheng, Y., Xu, R., Chang, S.-F., and Yuan, L. Learning visual representation from modality-shared contrastive language-image pre-training. In *Computer Vision – ECCV 2022*, pp. 69–87, 2022.

Yu, Q., Weber, M., Deng, X., Shen, X., Cremers, D., and Chen, L.-C. An image is worth 32 tokens for reconstruction and generation. *Advances in Neural Information Processing Systems*, 37:128940–128966, 2024.

Yu, Y., Chan, K. H. R., You, C., Song, C., and Ma, Y. Learning diverse and discriminative representations via the principle of maximal coding rate reduction. *Advances in neural information processing systems*, 33:9422–9434, 2020.

Zhang, B. H., Lemoine, B., and Mitchell, M. Mitigating unwanted biases with adversarial learning. In *Proceedings of the 2018 AAAI/ACM Conference on AI, Ethics, and Society*, pp. 335–340, 2018.

Zhang, R., Hao, X., Han, Y., Cao, J., Liu, Y., and Zhang, K. Mbcodec: Thorough disentangle for high-fidelity audio compression. *arXiv preprint arXiv:2509.17006*, 2025.

Zhang, Y., Yan, L., Qin, Z., Zhuang, H., Shen, J., Wang, X., Bendersky, M., and Najork, M. Towards disentangling relevance and bias in unbiased learning to rank. In *Proceedings of the 29th ACM SIGKDD Conference on Knowledge Discovery and Data Mining*, pp. 5618–5627, 2023.

Zhao, Y., Zhang, C., Huang, H., Li, H., and Zhao, Z. Towards effective multi-modal interchanges in zero-resource sounding object localization. In *Advances in Neural Information Processing Systems*, volume 35, pp. 38089–38102, 2022.

Zhou, J., Zheng, L., Zhong, Y., Hao, S., and Wang, M. Positive sample propagation along the audio-visual event line. In *Proceedings of the IEEE/CVF Conference on Computer Vision and Pattern Recognition (CVPR)*, pp. 8436–8444, June 2021.

Zhou, J., Guo, D., and Wang, M. Contrastive positive sample propagation along the audio-visual event line. *IEEE*

Transactions on Pattern Analysis and Machine Intelligence, 45(6):7239–7257, 2023. doi: 10.1109/TPAMI.2022.3223688.

A. Details of CMG Downstream Tasks

Pre-train Details:

Following the standard CMG evaluation protocol, we adopt the same backbone architectures as Unicode (Xia et al., 2023). Specifically, for each 1-second visual segment we uniformly sample 16 RGB frames and extract deep convolutional feature maps from VGG-19 after the final pooling stage; we then apply global average pooling across the 16 frames to obtain $7 \times 7 \times 512$ -D visual feature maps. For the audio stream, we employ a VGG-like network pre-trained on AudioSet to extract 128-D features for each 1-second audio segment. For both modalities, we further project semantic representations into a shared 512-D embedding space.

To capture modality-specific information, the video branch uses a convolutional encoder to produce spatial feature maps of shape $3 \times 3 \times 2048$; we apply spatial average pooling followed by a linear projection to obtain video-specific features of shape $T \times 512$. The audio branch uses a linear encoder to produce audio features of shape $T \times 256$. The video-specific features and audio features are used for reconstruction and for adversarial disentanglement via a GRL-based decoupler and Local Sliding Alignment. In contrast to prior unified-representation approaches (e.g., DCID (Huang et al., 2025), FCID (Huang et al., 2025)) that rely on additional text supervision, our Asymmetric Hierarchical Anchoring (AHA) framework is pre-trained solely on paired audio–video data in this downstream tasks.

For Cross-CPC, we set the prediction horizon to one step and apply it between the two modality semantic sequences during unified-representation pre-training. For GRL-based disentanglement, we first update the GRL discriminators once with frozen encoders, and then update the full model (encoder, CPC, decoder) with GRL reversal in the main pass. We use a learning rate of 1×10^{-4} , set $\gamma = 0.99$ for MM-EMA, and adopt a batch size of 96.

Details of all downstream tasks:

Table 6. Details of all downstream tasks.

Task	Pretrained Modality	Downstream Dataset	Generalization Direction
Cross-Modal Event Classification	Audio-Visual	AVE	$A \rightarrow V$ $V \rightarrow A$
Cross-Modal Event Localization	Audio-Visual	AVVP	$A \rightarrow V$ $V \rightarrow A$
Cross Modal & Dataset Event Localization	Audio-Visual	AVE & AVVP	$A(AVE) \rightarrow V(AVVP)$ $V(AVE) \rightarrow A(AVVP)$ $UCF(v) \leftrightarrow VGG(a)$

Cross-Modal Event Classification (AVE) (Tian et al., 2018): The AVE dataset contains 28 event categories and each audio/video clip is 10 seconds long. Given discrete representations extracted from one modality, we attach a two-layer MLP classifier to map the sequence into 28-way class logits, followed by a softmax and a standard cross-entropy loss. To test video-to-audio generalization ($V \rightarrow A$), we train the classifier using video-derived discrete sequences and then directly replace the input with audio-derived sequences at test time, keeping both the frozen encoder and the learned classifier unchanged; audio-to-video ($A \rightarrow V$) is evaluated analogously.

Cross-Modal Event Localization (AVVP) (Tian et al., 2020): The AVVP dataset includes 25 event categories, and a single clip may contain multiple events. We again use the frozen encoder to obtain a length- T discrete sequence, and employ a two-layer MLP localization head to predict 25-dimensional event scores (per segment). We apply a sigmoid activation and optimize with a multi-label classification objective (binary cross-entropy) against the ground-truth labels. All remaining training settings follow those used for cross-modal event classification.

Cross-Modal & Cross-Dataset Event Localization (AVE \rightarrow AVVP; UCF(v) \leftrightarrow VGG(a)): To further assess transferability across datasets, we consider the 12 overlapping event categories shared by AVE and AVVP: dog, car, helicopter, violin fiddle, frying food, motorcycle, acoustic guitar, banjo, baby cry, chainsaw, cat, accordion. We train the localization head using single-modality inputs from the AVE training set and directly evaluate on the opposite modality in the AVVP validation set, without any additional adaptation. Following prior practice, we report the F1 score as the primary metric, while keeping the optimization protocol identical to the AVVP localization setting. We also tested cross-modal classification tasks, performing classification between the visual modality on a subset of UCF-101 (Soomro et al., 2012) (16 classes) and the audio modality on a subset of VGGSound-AVEL (Zhou et al., 2021; 2023) (16 classes).

Brief Pipeline of symmetric structure:

Below is a schematic diagram of the symmetric structure in CMG Downstream Tasks and in the Talking Face Disentanglement Experiment. Except for slight differences in the peripheral structure (i.e., audio or video backbone, encoder, decoder), the main structure is shown in Figure 6.

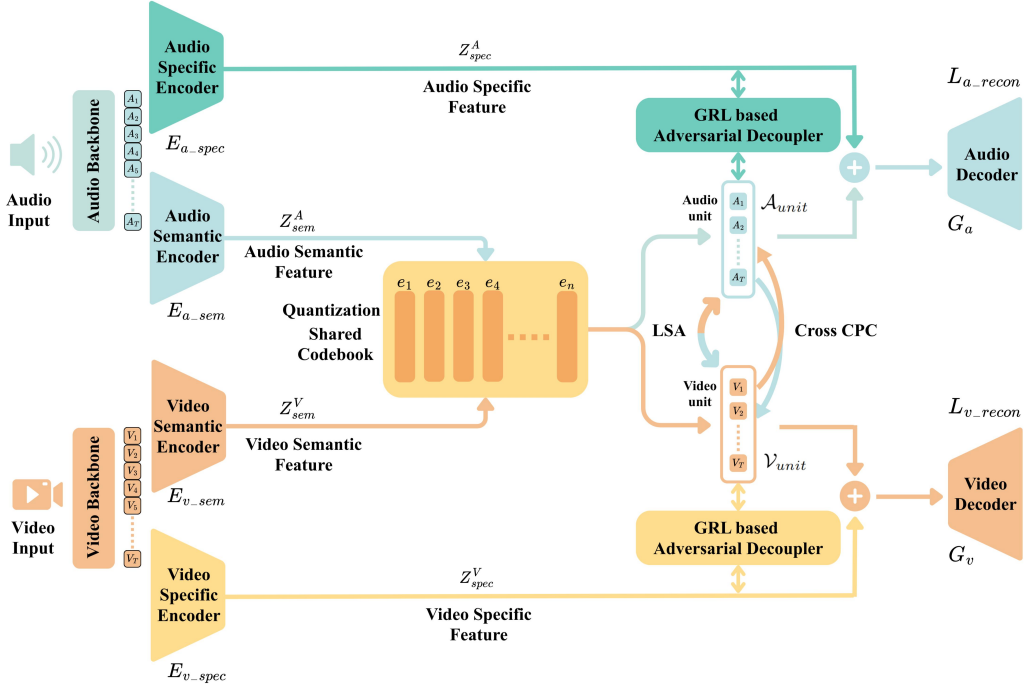


Figure 6. Brief Pipeline of symmetric structure

B. Details of Talking Face Disentanglement Experiment

Based on our initial AHA Pipeline, we replaced the Video backbone with LIA (Wang et al., 2022b; Ki et al., 2025) and the Audio Backbone with Wav2Vec2.0 (Baevski et al., 2020). The pipeline for the Talking-Face Disentanglement Experiment is shown in Figure 7(b). For the Video Backbone, LIA’s encoder extracts Identity Information from the input target image that represents identity of this image, and extracts Motion Information containing highly entangled facial features from it. We use this Motion Information as the video feature, with the detailed pipeline shown in Figure 7(a). Additionally, for the Audio Backbone, we used Wav2Vec to extract audio features. After processing with LIA and Wav2Vec, the final video input dimension and audio input dimension are both 512-D.

Specifically, for our decoupling process, we select a video not present in the training data as the Semantic Video. After passing through the Encoder of LIA, we obtain the Identity Information of Semantic Video and Motion Information of Semantic Video. Additionally, we select another video also not present in the training data as the Specific Video. After similarly passing through the Encoder of LIA, we obtain the Identity Information of Specific Video and Motion Information of Specific Video. We freeze the obtained Identity Information and input the Motion Information into our AHA, obtaining the Semantic Vector of Semantic Video, Semantic Vector of Specific Video, Specific Vector of Semantic Video, and Specific Vector of Specific Video respectively. Finally, we select the Semantic Vector of Semantic Video and Specific Vector of Specific Video, concatenate them, and send them to the Decoder to obtain the Decoupled Motion Information. Together with the frozen Identity Information of Semantic Video, we input them into the Renderer of LIA to finally obtain our Decoupled Talking-Face Video.

Therefore, the expected effect is to generate a fused Decoupled Talking-Face Video that combines the mouth movements obtained from the Semantic Video with the audio-independent motions (such as blinking actions) from the Specific Video.

For our training details, we selected a subset of the TalkVid (Chen et al., 2025a) dataset (approximately 38.4 hours). After our data processing, we ultimately used approximately 30.6 hours of data and trained for approximately 10 hours across 4 A6000 GPUs, covering 250 epochs.

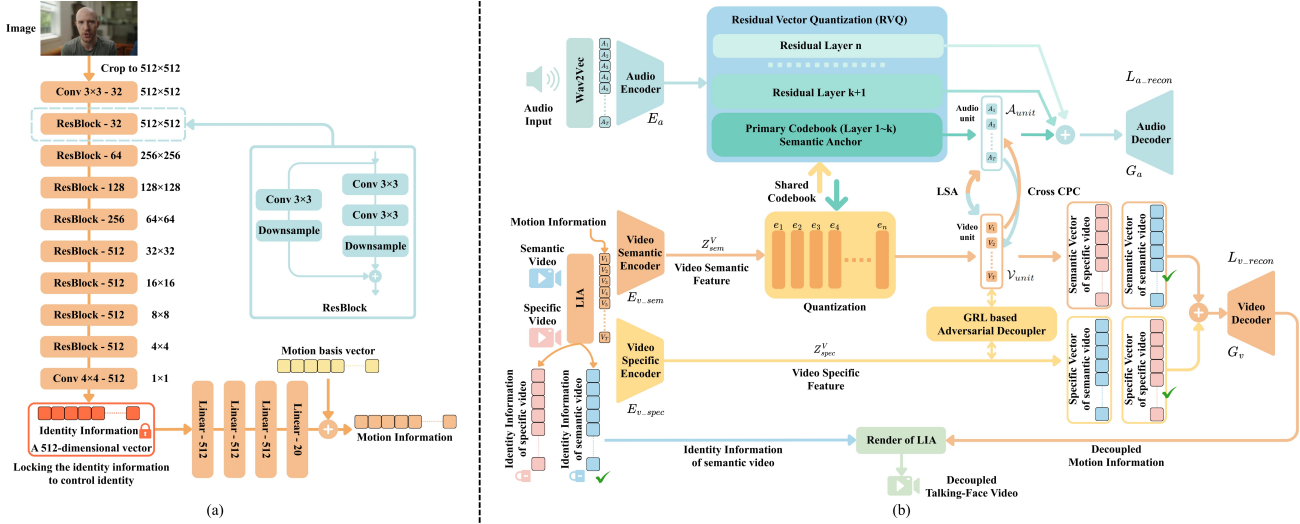


Figure 7. (a) LIA's Brief Pipeline for Extracting Identity Information and Motion Information; (b) Brief Pipeline for Talking Face Disentanglement Experiment

Data Processing Details:

1. Face Recognition: Due to transitions or narration in YouTube videos, TalkVid may contain video segments with audio but no actual human faces. Therefore, we used Face Recognition to detect whether the video contains human faces and removed videos without faces.
2. Silence Detection: Since some videos contain prolonged silence (exceeding 1/3 of the video duration), which is useless for training purposes, we also performed silence detection on the videos.
3. Audio-Visual Synchronization: Since most data in TalkVid comes from YouTube, some videos are similar to film reviews or commentary videos that contain facial action videos, but the audio and corresponding video cannot be properly synchronized. Based on this problem, we made certain adjustments based on the Python code from ([Chung & Zisserman, 2016](#)), and filtered out videos that meet our requirements for audio-visual synchronization.
4. Phoneme Extraction: To better demonstrate the modality transfer effect, consistent with the CMG experiment approach, we add a phoneme supervision on the audio shared RVQ that is very sparse in the time dimension (statistically around 20% of frames participate), i.e., adding a simple classification head to perform phoneme classification on labeled frames. We use BFA ([Rehman et al., 2025](#)) to extract phonemes.
5. Large Angle Face Detection: Since some videos contain significant angle changes in face orientation, mouth information may be lost due to large-angle movements, which affects our experiments. Therefore, we used ([Hempel et al., 2022](#)) to detect large angles in videos and removed videos where face rotation exceeds 60 degrees from the dataset.

More Talking Face Disentanglement Experiment Examples:

More experimental results can be found in [Figure 9](#) and [Figure 10](#). From the extensive experimental results, we can see the robustness of our model in terms of decoupling stability and reconstruction fidelity.

Detailed diagrams of PCA and UMAP:

To more clearly see the individual distribution of specific features and semantic features respectively, we present the PCA and UMAP details of specific feature only and semantic feature only in [Figure 8](#).

Evaluation Metrics:

1. **PSNR (Horé & Ziou, 2010):** Peak Signal-to-Noise Ratio (PSNR) measures the reconstruction quality of an image by comparing it with the reference image, higher values indicate better fidelity.

2. **LPIPS** (Zhang et al., 2018): Learned Perceptual Image Patch Similarity (LPIPS) is used to measure the perceptual similarity between reconstructed image and real image based on the pre-trained AlexNet features.
3. **V2V-LS (Ours)**: We propose a video-to-video lip-sync metric inspired by Wav2Lip (Prajwal et al., 2020), using visual embeddings from AV-HuBERT (Shi et al., 2022). The lip region embeddings of the two videos are compared via frame-wise differences to compute a score, quantifying how well the source video drives the target lip movements.
4. **Mouth RMSE**: Root-mean-square error (RMSE) computed over the 2D mouth landmarks of two videos, capturing frame-wise geometric misalignment of the lips; lower values indicate better lip synchronization.

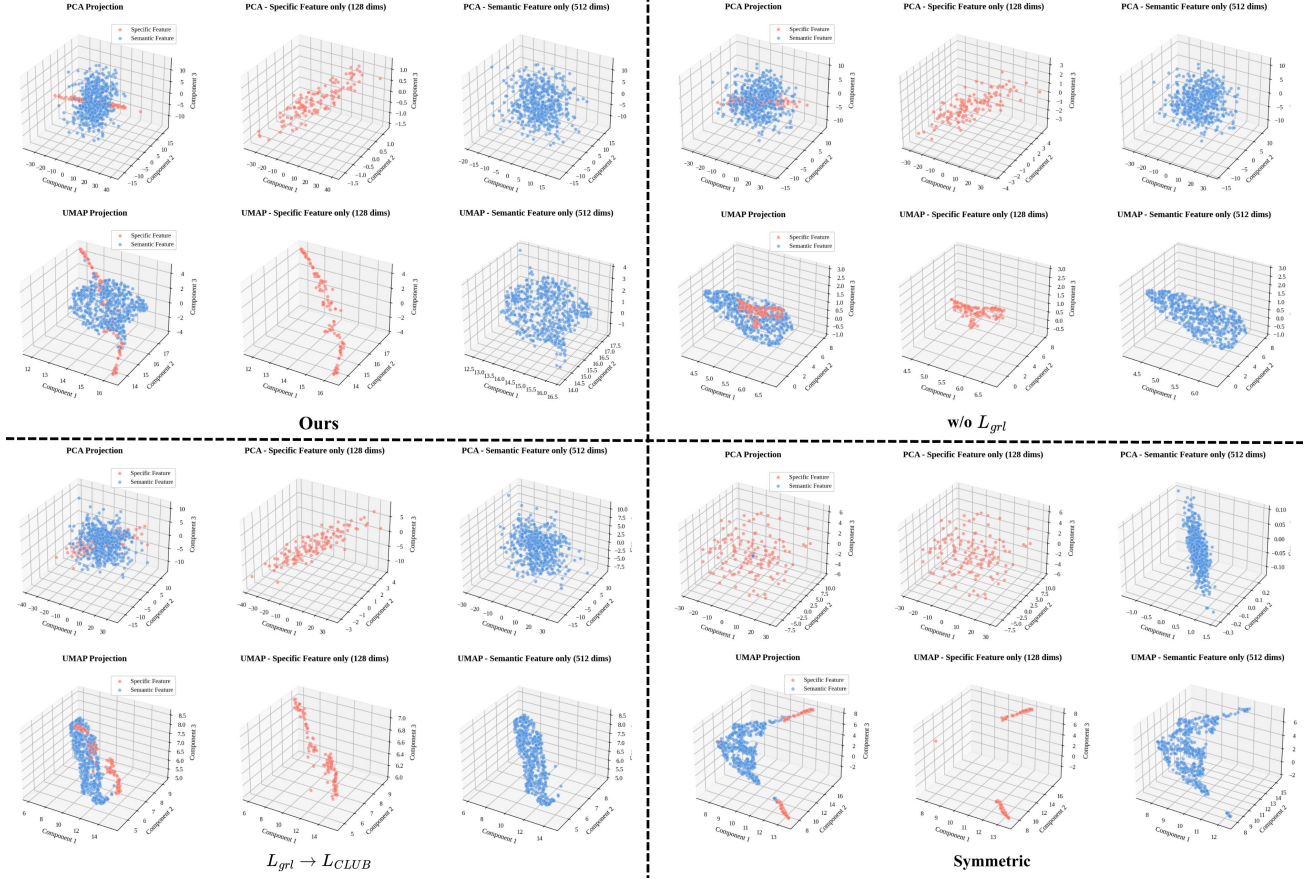


Figure 8. Detailed diagrams of PCA and UMAP

C. Training Details

Table 7 shows a portion of the hyperparameters used during our training process and their corresponding values. Figure 11 shows the GRL loss during our training process. As can be seen, after a certain number of steps, the GRL loss stabilizes and fluctuates around 4.28. This value is determined by $\ln(\text{batchsize} \times \text{GRL negative sample ratio}) = \ln(96 \times 0.75) = 4.28$ in our experiment. Fluctuations around this value indicate that the GRL adversarial process is proceeding normally during our model training.

Training Efficiency: All models were trained for 250 epochs on 4 NVIDIA A6000 GPUs with batch size 96. Our proposed AHA completed training in approximately **9.7** hours, while symmetric structure required **13.3** hours, demonstrating a **27%** improvement in training efficiency.

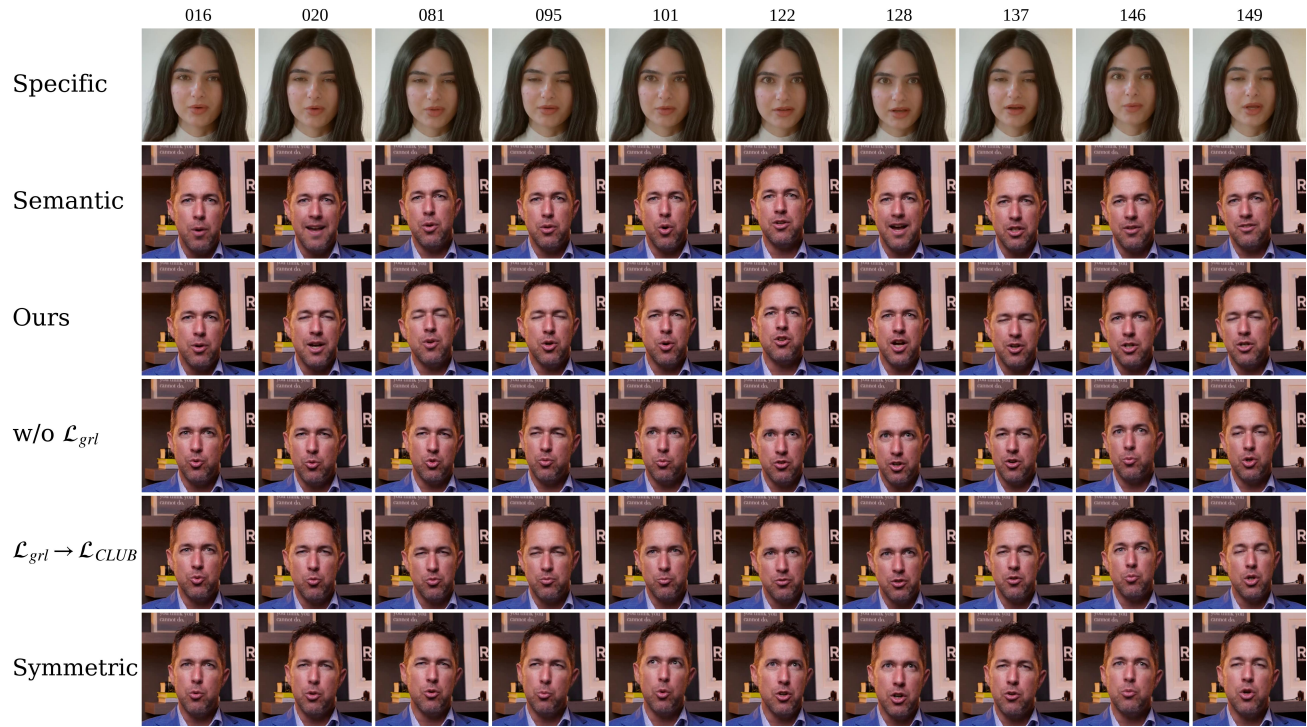


Figure 9. More Talking Face Disentanglement Experiment Examples (1)

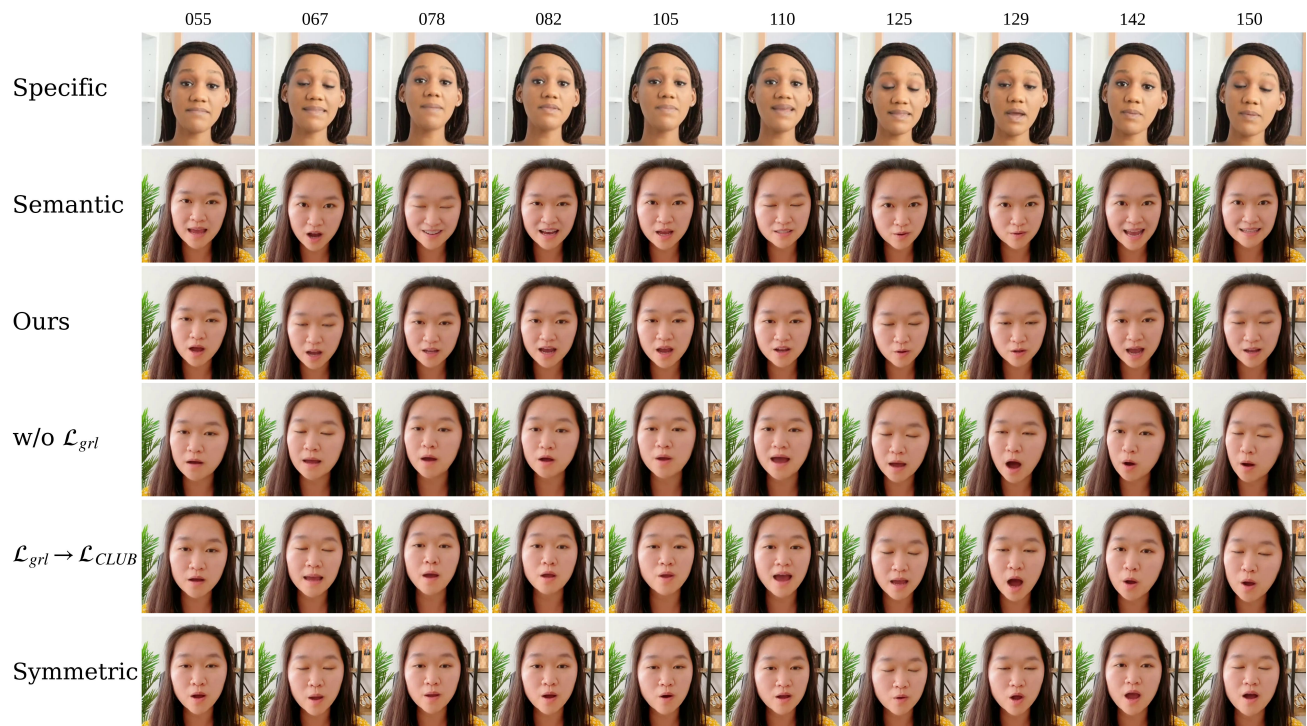


Figure 10. More Talking Face Disentanglement Experiment Examples (2)

Table 7. Some hyperparameters and their values.

Hyperparameter	Value	Hyperparameter	Value
Codebook size	512	Embedding dimension	512
CPC hidden dimension	256	CPC context dimension	256
CPC LSTM layers	2	CPC prediction steps	1
GRL velocity sample ratio	0.4	GRL negative sample ratio	0.75
Main optimizer	AdamW	GRL optimizer	Adam (learning rate = 1e-4)
Learning rate scheduler	CosineAnnealingWarmupLR	Warmup epochs	5
Minimum learning rate	1e-6	GRL temperature ratio τ	0.1
GRL λ_{max}	1	Audio extra layers	3
Positive tolerance set(CMG Tasks)	1	Positive tolerance set(Talking Face Experiment)	3
LSA window size(CMG Tasks)	5	LSA window size(Talking Face Experiment)	31
Shared RVQ Layers (CMG Tasks)	1	Shared RVQ Layers (Talking Face Experiment)	2

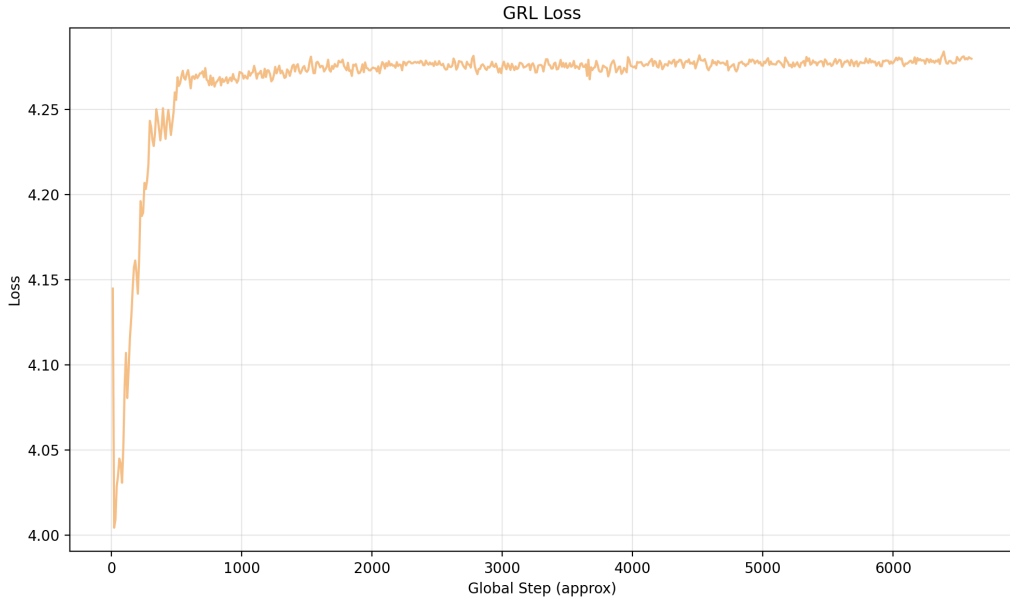


Figure 11. Changes in GRL Loss During Training